

## Effect of partition coefficient on microsegregation during solidification of aluminium alloys

M.H. Avazkonandeh-Gharavol<sup>1)</sup>, M. Haddad-Sabzevar<sup>1)</sup>, and H. Fredriksson<sup>2)</sup>

1) Department of Metallurgy and Materials Engineering, Faculty of Engineering, Ferdowsi University of Mashhad, Azadi Square 91775-1111, Mashhad, Iran

2) Department of Materials Science and Engineering, School of Industrial Engineering and Management, Royal Institute of Technology, Brinellvägen 23, Stockholm 100 44, Sweden

(Received: 11 December 2013; revised: 8 March 2014; accepted: 15 April 2014)

**Abstract:** In the modeling of microsegregation, the partition coefficient is usually calculated using data from the equilibrium phase diagrams. The aim of this study was to experimentally and theoretically analyze the partition coefficient in binary aluminum–copper alloys. The samples were analyzed by differential thermal analysis (DTA), which were melted and quenched from different temperatures during solidification. The mass fraction and composition of phases were measured by image processing and scanning electron microscopy (SEM) equipped with an energy-dispersive X-ray spectroscopy (EDS) unit. These data were used to calculate as the experimental partition coefficients with four different methods. The experimental and equilibrium partition coefficients were used to model the concentration profile in the primary phase. The modeling results show that the profiles calculated by the experimental partition coefficients are more consistent with the experimental profiles, compared to those calculated using the equilibrium partition coefficients.

**Keywords:** aluminum copper alloys; solidification; partition coefficient; microsegregation; numerical modeling; differential thermal analysis

### 1. Introduction

Microsegregation, which is the non-uniform distribution of alloying elements in the scale of dendrite arm spacing (DAS), is one of the most important phenomena during solidification. It usually results in the formation of some unexpected secondary phases that, in general, reduces the workability of casting products. Because of its industrial importance, microsegregation has been extensively studied both theoretically and experimentally during the last decades, and several models have been developed to predict the microsegregation with different degrees of accuracy [1–11].

The main reason of microsegregation is the thermodynamics of solidification, and hence, the partition coefficient ( $k_0$ ) is defined as [12–13]

$$k_0 = \frac{C_S^i}{C_L^i} \quad (1)$$

where  $C_S^i$  and  $C_L^i$  are the concentrations of solute atoms

in solid and liquid at the interface, respectively. In most cases,  $k_0 < 1$  and the alloying elements prefer to remain in the liquid during solidification; the concentration of alloying elements thus increases in the liquid during solidification. In most binary alloys, depending on the situation and conditions, such as the composition or cooling rate, the liquid composition may reach the eutectic composition. Thus, some non-equilibrium eutectic phases can also be formed even in very dilute alloys that should be solidified as a single phase alloy.

The two basic models for analysis of solidification process are the equilibrium and non-equilibrium lever rules, which are simply referred to as “the lever rule” and “the Scheil equation”, respectively. These models are still widely used in the literature to compare with theoretical and/or experimental results. The lever rule and the Scheil equation show the lower and upper boundaries for microsegregation, respectively. The Scheil equation is defined as

$$C_S^i = C_0 k_0 (1 - f)^{-(1-k_0)} \quad (2)$$

where  $C_0$  and  $f$  are the nominal composition and the solid

Corresponding author: M.H. Avazkonandeh-Gharavol E-mail: mhgharavol@gmail.com

© University of Science and Technology Beijing and Springer-Verlag Berlin Heidelberg 2014

mass fraction of alloy, respectively. Through the electron probe microanalysis (EPMA) was used, the inaccuracies of these models were elucidated, and some corrections were implemented to achieve a better correlation with experimental results. The main corrections included the considerations of back diffusion, coarsening, and undercooling [4,9–11]. Though the extensive efforts have been devoted to this field, some discrepancies remain between theoretical calculations and experimental results. In recent years, some researchers have noted that these errors may arise from the use of inaccurate data in models, such as the erroneous diffusion and partition coefficients. Xie *et al.* [14–16] and Kurum *et al.* [17] explored some new data related to the Al–Cu phase diagram and diffusion coefficient, and used them to model the microsegregation in binary Al–Cu alloys. They showed that, with these new data, a better correlation with experimental results could be achieved.

The study of microsegregation can be divided in three topics: the physical basis, the modeling process, and the data used in modeling. The first two topics have been extensively studied in the literature. However, the data that are typically used in modeling are taken from very old references and may not be sufficiently accurate, which can cause some errors in calculations. Most of the thermodynamic data extracted from phase diagram, such as  $k_0$ , is applicable for the equilibrium conditions and not for the practical situations. Therefore, the aim in this investigation was to experimentally measure the  $k_0$  value for binary Al–Cu alloys. The equilibrium ( $k_0^{\text{Eq}}$ ) and experimental ( $k_0^{\text{Exp}}$ ) partition coefficients were used to calculate the concentration profile across the secondary dendrite arms. The calculated profiles were then compared to experimental profiles, and the origin of discrepancies was discussed.

## 2. Experimental

### 2.1. Sample preparation

Al–Cu alloys containing 2.2wt%, 3.7wt%, and 4.8wt% Cu were selected as model binary alloys and prepared from the high-purity starting materials. The chemical composition of the alloys was determined by conventional spark emission spectroscopy. For experimental examination of  $k_0$ , differential thermal analysis (DTA) with quenching during solidification was used. For this purpose, approximately 1 g of each alloy was melted, heated to approximately 50°C above its melting temperature, and then cooled at a cooling rate ( $R$ ) of 0.5 or 5 K·min<sup>-1</sup>. The samples were quenched from different temperatures during cooling. In each set of experiments, one sample was quenched immediately after the end of solidification. The sample codes and quenching tempera-

tures are listed in Table 1.

### 2.2. Microstructure characterization

The structure of samples quenched during solidification can be divided into two parts, the first part contains the coarse primary  $\alpha$ -Al dendrites formed before quenching, and the second part consists of very fine primary dendrites and eutectic phases formed during quenching. Hereafter, the first part was referred to as the “primary phase” and the second part as the “quenched melt”. The samples were prepared for microstructural and compositional analysis by the conventional methods. The mass fraction of phases was determined by the manual Swift point-counting method based on standard ASTM E562-11. To achieve the reasonable precision, more than 2000 points were counted. The lowest magnification at which the phases could be clearly distinguished was used.

### 2.3. Scanning electron microscopy (SEM) analysis

The chemical composition of quenched melt ( $C_L$ ) and the concentration profile in the solid were determined by scanning electron microscopy and energy-dispersive X-ray spectroscopy (SEM/EDS). The EDS detector was first calibrated using the standard samples contained 3wt%, 6wt%, and 10wt% Cu. The chemical composition of quenched melt during solidification was measured by SEM/EDS areal analysis, as shown in Fig. 1(a). For each sample, at least five regions were selected and analyzed, and their average value was reported as  $C_L$ . For some of the samples, the concentration profile in the primary phase was measured by SEM/EDS point analysis. To achieve a statistically significant concentration profile in the solid, approximately 100 points were selected and analyzed by SEM/EDS, as shown in Fig. 1(b). These data were processed on the basis of the method proposed by Gungor [18] to obtain the concentration profile.

### 2.4. Analysis of partition coefficients

Partition coefficients ( $k_0^{\text{Exp}}$ ) were calculated by four different methods, as described below. In the first method (M1), the experimentally measured  $C_L$  and the mass fraction of quenched melt ( $f_L$ ) were substituted into the Scheil equation (Eq. (3)) to estimate the value of  $k_0$  ( $k_0^{\text{Exp-1}}$ ). In the second method (M2), the measured  $C_L$  and  $f_L$  were used as input data in the lever rule to calculate  $k_0$  ( $k_0^{\text{Exp-2}}$ ) according to Eq. (4). In the third method (M3), the minimum concentration of Cu was measured from SEM/EDS point analysis in the primary phase, and the value of  $k_0$  ( $k_0^{\text{Exp-3}}$ ) was calculated from Eq. (5). In the fourth method (M4), the Scheil equation was

**Table 1. Thermal analysis parameters and experimental results**

Sample code	$C_0$ / wt%	$R$ / (K·min <sup>-1</sup> )	$T_L$ / °C	$T_q$ / °C	$C_L$ / wt%		$C_{min}$ / wt%	$f_s$ / wt%		SDAS / μm
					Eq.	Exp.		Eq.*	Exp.	
22CuS1	2.2	0.5	653	645	6.1	5.7	0.28	71.8	81.2	153.6
22CuS2	2.2	0.5	653	640	7.8	9.6	0.43	81.4	91.6	164.5
22CuS3	2.2	0.5	653	615	15.9	16.8	0.59	99.4	95.7	220.5
22CuS4	2.2	0.5	653	570	27.8	27.2	0.72	100	98.9	306.8
22CuSF	2.2	0.5	653	530	—	—	1.08	100	99.8	326.8
22CuM1	2.2	5	650	645	6.1	3.2	0.30	71.8	75.1	64.5
22CuM2	2.2	5	650	640	7.8	5.8	0.40	81.4	81.5	91.7
22CuM3	2.2	5	650	615	15.9	18.0	0.40	99.4	94.0	110.2
22CuM4	2.2	5	650	570	27.8	32.8	0.53	100	97.0	121.4
22CuMF	2.2	5	650	530	—	—	0.55	100	99.0	122.7
37CuS1	3.7	0.5	648	640	7.8	8.1	0.64	59.7	69.2	133.7
37CuS2	3.7	0.5	648	635	9.5	10.1	0.80	69.5	79.2	154.5
37CuS3	3.7	0.5	648	615	15.9	21.4	1.16	88.5	93.2	186.9
37CuS4	3.7	0.5	648	570	27.8	31.5	1.21	100	95.3	265.5
37CuSF	3.7	0.5	648	530	—	—	1.72	100	96.5	269.5
37CuM1	3.7	5	646	640	7.8	5.3	0.56	59.7	59.6	66.1
37CuM2	3.7	5	646	635	9.5	9.1	0.75	69.5	75.9	77.3
37CuM3	3.7	5	646	615	15.9	23.2	0.75	88.5	90.0	101.3
37CuM4	3.7	5	646	570	27.8	31.0	1.05	100	92.6	113.0
37CuMF	3.7	5	646	530	—	—	0.98	100	95.5	122.4
48CuS1	4.8	0.5	646	635	9.5	9.4	0.98	56.4	69.2	134.0
48CuS2	4.8	0.5	646	630	11.2	11.9	1.06	65.2	77.0	144.5
48CuS3	4.8	0.5	646	615	15.9	19.1	1.32	80.5	88.7	176.1
48CuS4	4.8	0.5	646	570	27.8	32.2	1.72	98.5	93.1	233.4
48CuSF	4.8	0.5	646	530	—	—	1.95	100	95.7	263.7
48CuM1	4.8	5	643	635	9.5	8.3	0.73	63.6	63.4	69.3
48CuM2	4.8	5	643	630	11.2	10.0	0.85	71.4	71.2	83.2
48CuM3	4.8	5	643	615	15.9	17.5	0.94	81.9	81.6	96.9
48CuM4	4.8	5	643	570	27.8	32.3	1.11	92.8	92.8	108.3
48CuMF	4.8	5	643	530	—	—	1.43	100	95.0	106.2

Note:  $T_L$  represents the liquidus temperature,  $T_q$  the quenching temperature,  $C_L$  the composition of the quenched melt,  $C_{min}$  the minimum concentration in primary phase,  $f_s$  the solid fraction, SDAS the secondary dendrite arms spacing, and \* calculated based on the lever rule.

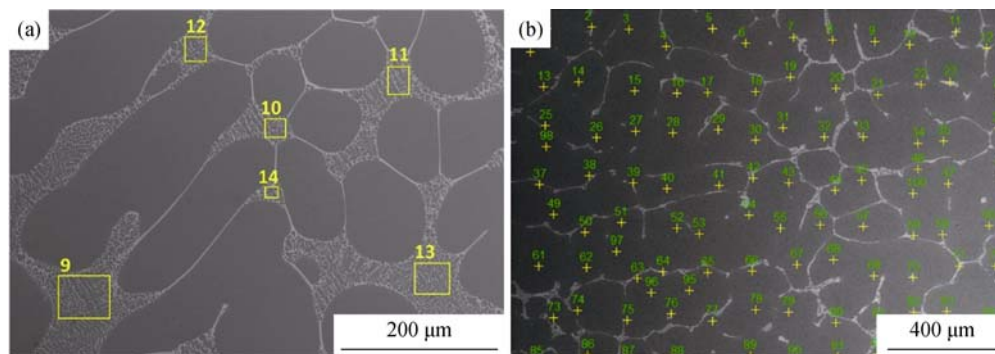


**Fig. 1. Measurement of the chemical composition of quenched melt and the concentration profile of primary phase by SEM/EDS: (a) areal analysis of 48CuM2; (b) point analysis of 48CuMF.**

fitted to the experimental concentration profile using the least-squares method with  $k_0$  treated as a free parameter ( $k_0^{\text{Exp-4}}$ ), according to the procedure developed by Valdes *et al.* [19].

$$k_0^{\text{Exp-1}} = 1 + \frac{\ln(C_L/C_0)}{\ln(f_L)} \quad (3)$$

$$k_0^{\text{Exp-2}} = \frac{C_0 - C_L f_L}{1 - f_L} \quad (4)$$

$$k_0^{\text{Exp-3}} = \frac{C_{\min}}{C_0} \quad (5)$$

## 2.5. Modeling

The  $k_0^{\text{Exp}}$  values calculated using different methods and the  $k_0^{\text{Eq}}$  value were used in a model to calculate the concentration profile in the primary phase, considering back diffusion and coarsening. An iterative method was used to calculate the concentration profile in the solid [13], as shown in Eq. (6).

$$C_s(f, t) = C_s^i - (C_s^i - C_{\min}) \exp\left(-\frac{\pi^2 D_s}{f_0^2 d^2} t\right) \cos\left(\frac{\pi f}{2 f_0}\right) \quad (6)$$

where  $C_s(f, t)$  is the concentration profile in the primary phase at time  $t$ ,  $f$  the solid fraction,  $C_{\min}$  the minimum concentration at the center of the primary phase,  $D_s$  the diffusion coefficient in the solid,  $d$  the secondary dendrite arm spacing (SDAS), and  $f_0$  the solid fraction at time  $t$ . Before Eq. (6) is used, the solidification range (from  $T_{\text{start}}$  to  $T_{\text{finish}}$ ) should be divided into several intervals ( $\Delta T_i$ ). Time and temperature are related to the cooling scheme, for example, each temperature interval corresponds to a specific time. The values of  $C_{\min}$  and  $f_0$  should be estimated for each temperature interval (or equivalent time). The preliminary value of  $f_0$  can be calculated with the aid of mass balance according to Eq. (7). For this purpose, it is assumed that  $t = 0$  and  $C_{\min} = C_0 \times k_0$ .

$$(C_L^i - C_0)(1 - f_0) = \int_0^{f_0} \left[ C_0 - C_s^i + (C_s^i - C_{\min}) \exp\left(-\frac{\pi^2 D_s}{f_0^2 d^2} t\right) \cos\left(\frac{f \pi}{2 f_0}\right) \right] df \quad (7)$$

The true value of  $f_0$  at  $t = 0$  is zero, and the preliminary value of  $f_0$  is simply a starting value for the calculation of  $f_0'$ . In the next step, for the first temperature interval ( $\Delta T_1$  or the equivalent time  $t_1$ ), a better estimation of  $C_{\min}$  is achieved by Eq. (6), assuming that  $f = 0$  and  $C_{\min} = C_0 \times k_0$  ( $C_{\min}' = C_s(0, t)$ ). The calculations by Eqs. (6) and (7) are then repeated using the new values of  $f_0$  and  $C_{\min}$  ( $C_{\min}'$ ) as input parameters. If the difference between the calculated

values ( $f_0'$  and  $C_{\min}''$ ) and the previously calculated values ( $f_0$  and  $C_{\min}'$ ) is considerable, then the calculation should be repeated again with the new values as input data ( $f_0'$  and  $C_{\min}''$ ) until the difference between the newly calculated values and the previous ones becomes negligible. After  $f_0$  and  $C_{\min}$  are calculated, Eq. (6) can be used to calculate the concentration profile in the primary phase. More details about the implementation of the model are referred to Ref. [13]. Two sets of thermodynamic data, i.e., equilibrium data from the phase diagram and experimentally measured data in this study, were used to calculate the concentration profile. Diffusion data were extracted from the work of Gale and Totemeier [20]. The comparison between the calculated and experimental profile and the origin of discrepancies were discussed in the subsequent section.

## 3. Results and discussion

The chemical composition of the alloys is shown in Table 2. Only minor amounts of Si and Fe are present as impurities in the alloys. These impurities form a negligible, needle-shaped phase in the samples quenched after the end of solidification. The cooling curves for Al-4.8wt%Cu alloy cooled at 5 K·min<sup>-1</sup> are shown in Fig. 2(a). Arrows in the figure indicate the quenching temperatures. The solidification start temperature ( $T_L$ ) is reported in Table 1. In Fig. 2(b), the DTA curve for sample 48CuMF is shown. Three peaks can be distinguished in the curve. The first peak shows the beginning of the  $\alpha$ -Al phase solidification, the second peak is very small and is related to the solidification of the Fe-rich phase, and the last peak indicates the eutectic solidification. The same peaks were observed in the DTA curves of 37Cu alloy cooled at either rate. In the case of 22Cu alloy, the eutectic solidification peak was not observed in the DTA curve at either cooling rate; however, the eutectic structure was still present. This lack of an observed eutectic solidification peak may be due to the low sensitivity of DTA instrument, because the volume fraction of the eutectic phase in 22Cu samples, which are demonstrated in the next section, is very small. The eutectic start temperatures were 543°C and 539°C for cooling rates of 0.5 and 5 K·min<sup>-1</sup>, respectively, for all of the alloys.

### 3.1. Microstructure characterization

The quantitative metallography results are presented in Table 1. The microstructures of Al-4.8wt%Cu samples quenched during solidification are presented in Fig. 3 as an example of the quenched structure. According to results in Table 1 and Fig. 3, the solid mass fraction increases

Table 2. Chemical composition of the used alloys

Alloy	Cu	Si	Fe	Mn	Mg	Zn	Ti	Cr	Ni	Pb	Sn	Ca	Al
22Cu	2.2	0.05	0.07	0.004	0.007	0.002	0.004	0.001	0.001	0.002	0.005	0.002	Bal.
37Cu	3.7	0.04	0.06	0.004	0.002	0.003	0.003	0.001	0.002	0.003	0.006	0.001	Bal.
48Cu	4.8	0.05	0.06	0.004	0.019	0.002	0.004	0.003	0.003	0.004	0.009	0.003	Bal.

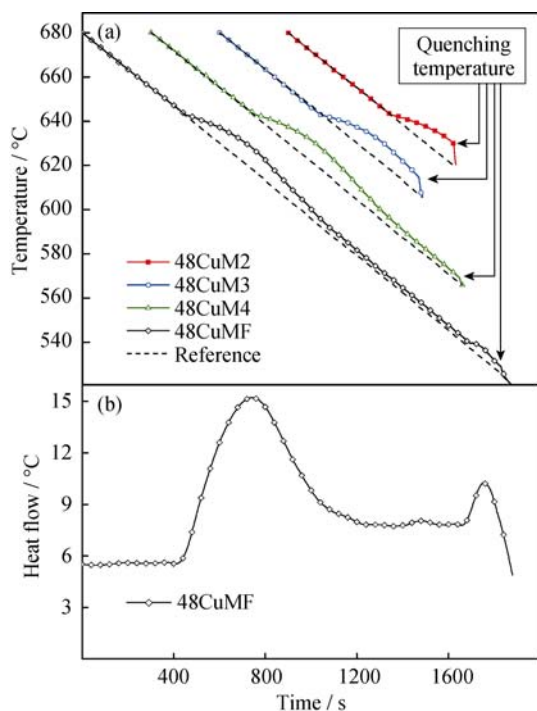


Fig. 2. Cooling curves for Al-4.8wt%Cu cooled at  $5 \text{ K}\cdot\text{min}^{-1}$  (a) and DTA curve of 48CuMF sample (b).

continuously with decreasing quenching temperature. On the basis of data in Table 1, the equilibrium values are reasonably less than the experimental values at high temperatures. As the solidification continues, the equilibrium values increase more rapidly than the experimental values, and the

experimental values will be less than the equilibrium values at the end of solidification. These deviations from equilibrium should be discussed in terms of the change in the equilibrium phase diagram, which are addressed later. Some of the quenching temperatures, such as 615 and 570°C, are common among different alloys. The solid fraction is reduced at these common quenching temperatures with the increase in cooling rate and copper content of the alloy. The reduction of solid fraction is caused by the undercooling effect associated with the increase of cooling rate and element content of the alloy. The structures of samples quenched after the end of solidification are shown in Fig. 4. With the increase of cooling rate, the microstructure becomes finer in the same alloys, as expected. In addition, at the same cooling rate, and the increase in the Cu content results in a finer microstructure.

### 3.2. SEM analysis

The results of SEM/EDS analysis are presented in Table 1 and Fig. 5. On the basis of data reported in Table 1, as the solidification proceeds, the  $C_L$  value increases monotonically. In contrast to the  $f_S$  values, the experimental values of  $C_L$  are lower than the equilibrium values at the beginning of solidification, and then increase to higher levels at the end of solidification. With decreasing quenching temperature, the  $C_{\min}$  value increases monotonically as a result of back diffusion.

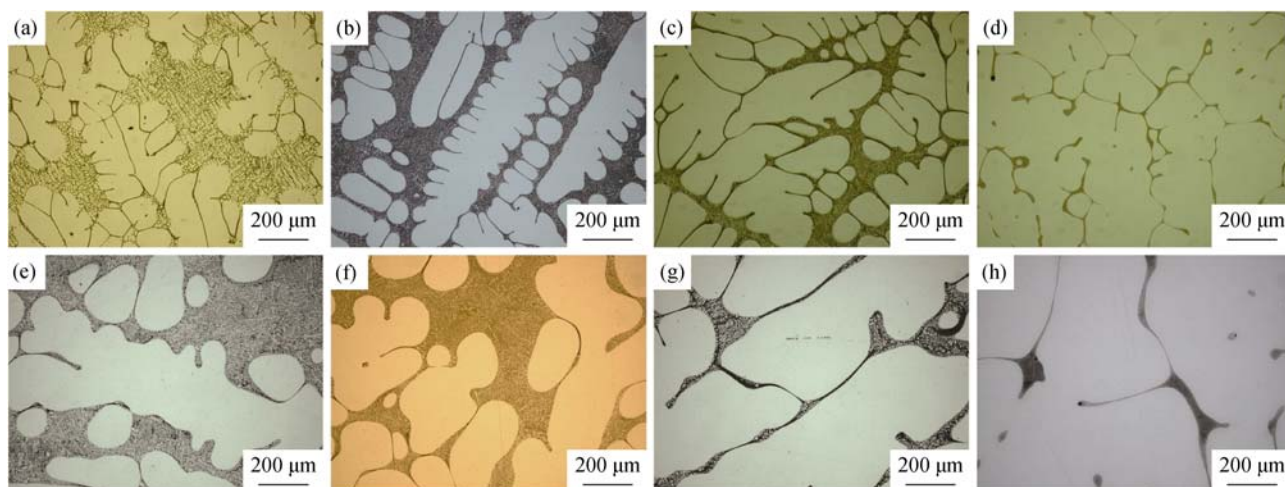


Fig. 3. Microstructures of quenched 48Cu samples: (a) 48CuM1; (b) 48CuM2; (c) 48CuM3; (d) 48CuM4; (e) 48CuS1; (f) 48CuS2; (g) 48CuS3; (h) 48CuS4.

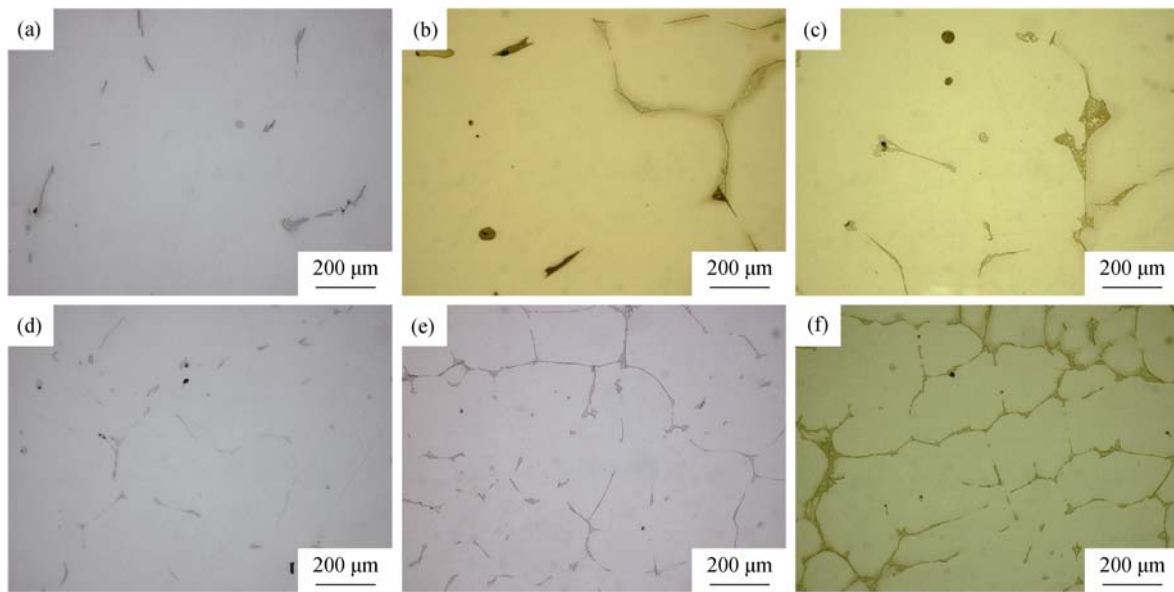


Fig. 4. Microstructures of samples quenched after the end of solidification: (a) 22CuSF; (b) 37CuSF; (c) 48CuSF; (d) 22CuMF; (e) 37CuMF; (f) 48CuMF.

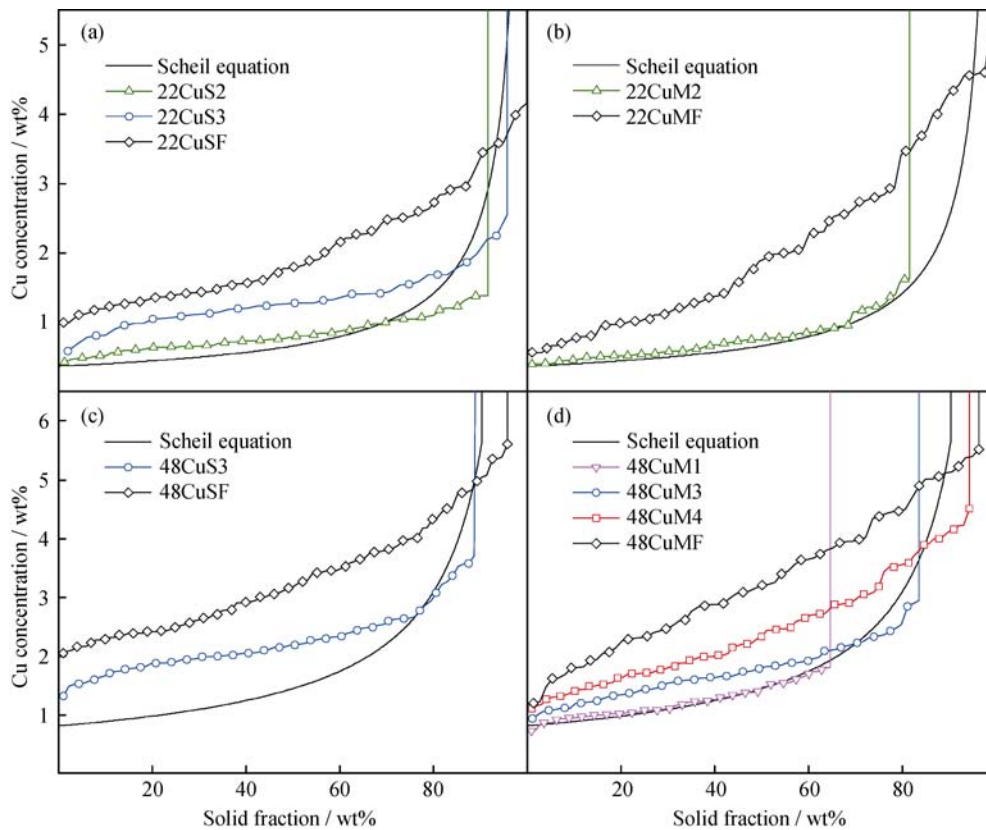


Fig. 5. Experimental concentration profile in the primary ( $\alpha$ -Al) phase: (a) 22CuS; (b) 22CuM; (c) 48CuS; (d) 48CuM.

This curve was calculated by Eq. (2), and  $k_0$  was assumed to be 0.17. The calculation result by the Scheil equation was also included in Fig. 5 for comparison. As shown in Fig. 5, the profile moves upward as the solidification proceeds. At

the early stages of solidification, a good agreement exists between the experimental concentration and the results from the Scheil equation, because the back diffusion does not yet have sufficient time to occur. However, as the solidification

continues, the difference between the experimental data and the results from the Scheil equation increases, so that, at the end of solidification, the results from experiment and the Scheil equation deviate. This deviation results from the back diffusion during solidification, which appears to be more important at the end of solidification because of a very high concentration gradient at the solid/liquid interface.

### 3.3. Analysis of partition coefficients

The results of  $k_0$  value are presented in Table 3 and Fig. 6. It can be seen that, most of the experimental results are much higher than the equilibrium values. Different trends can be observed for  $k_0$  values as a function of temperature in the different measurement methods. For M1, with the decrease of temperature, the  $k_0$  value first decreases and then increases. For M2, the  $k_0$  value decreases monotonically with decreasing temperature. For M3 and M4, the  $k_0$  value increases monotonically with decreasing temperature. The first two trends are likely not valid because of the inaccurate determinations of the quenched melt composition ( $C_L$ ) or the mass fraction ( $f_L$ ) of samples quenched from high temperatures. The mass fraction of melt in these samples is very high, and the extensive dilution occurs with the surrounding melt. In particular, the primary phase can move during quenching, which may also increase the level of dilution. Thus, the measured value for  $C_L$  is likely less than the true value, and the value of  $k_0$  is therefore overestimated. As the

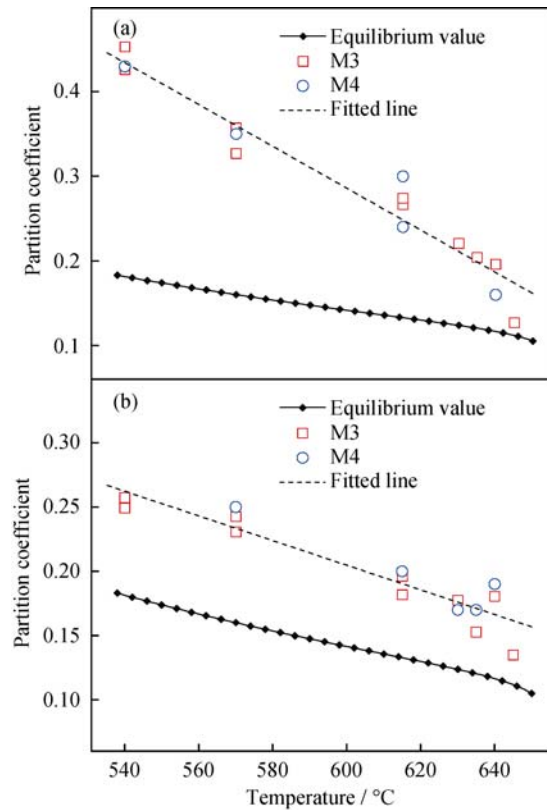


Fig. 6. Experimental and equilibrium values of  $k_0$  at different cooling rates: (a)  $0.5 \text{ K}\cdot\text{min}^{-1}$ ; (b)  $5 \text{ K}\cdot\text{min}^{-1}$ .

solidification continues, the determination accuracy of the melt composition and fraction increases; thus, the lower-temperature M1 results in the same trend observed for M3 and M4. With respect to the application of the lever rule, an additional complexity arises because of the relationship between the results and phase diagram. The deviation from equilibrium data is also observed in the cases of  $C_L$  and  $f_S$  (in Table 1). At  $615^\circ\text{C}$ , however, the equilibrium  $C_L$  and  $f_S$  values show the good agreement with the experimental results and, thus, so do the value of  $k_0$  at this temperature. At other temperatures, however, where the greater differences exist between the equilibrium values of  $C_L$  and  $f_S$  and their experimental values, the  $k_0$  value also deviates from the equilibrium  $k_0$  value. The achievement of better results by this method may first require the non-equilibrium phase diagram to be established. This project is currently underway, and the results will be published at a later date.

For M3 and M4, the  $k_0$  values are calculated on the basis of solid composition, which is not affected by the quenching process. The calculated values according to these two methods agree very well, and the trend is the same as the equilibrium trend; however, the values are noticeably higher than the equilibrium values. The  $k_0$  value calculated via M3 and M4 as well as the equilibrium values from the phase

Table 3. Results of  $k_0$  for 22Cu and 48Cu alloys

Sample code	$k_0$ by four different methods				Equilibrium value of $k_0$
	M1	M2	M3	M4	
22CuS1	0.43	0.25	0.13	—	0.11
22CuS2	0.40	0.16	0.20	0.16	0.12
22CuS3	0.35	0.09	0.27	0.30	0.13
22CuS4	0.44	0.07	0.33	0.51	0.16
22CuSF	—	—	0.49	0.59	0.17
22CuM1	0.73	0.59	0.14	—	0.11
22CuM2	0.42	0.24	0.18	0.19	0.12
22CuM3	0.26	0.07	0.18	—	0.13
22CuM4	0.23	0.04	0.24	0.48	0.16
22CuMF	—	—	0.25	0.51	0.17
48CuS1	0.43	0.29	0.20	—	0.12
48CuS2	0.38	0.22	0.22	—	0.12
48CuS3	0.37	0.16	0.27	0.24	0.13
48CuS4	0.29	0.09	0.36	0.35	0.16
48CuSF	—	—	0.41	0.43	0.17
48CuM1	0.46	0.34	0.15	0.17	0.12
48CuM2	0.41	0.27	0.18	0.17	0.12
48CuM3	0.24	0.11	0.20	0.20	0.13
48CuM4	0.27	0.08	0.23	0.25	0.16
48CuMF	—	—	0.30	0.39	0.17

diagram are shown in Fig. 6. As evident from the equilibrium data (except for those at very high temperatures), the  $k_0^{Eq}$  value linearly changes with temperature. Therefore, a line can be reasonably fit to the experimental data to determine the  $k_0^{Exp}$  value for each cooling rate at any composition and temperature. The data in Table 3 from 22Cu and 48Cu were used to fit the line. To achieve a more reliable fit, the data from both methods were used to fit a line to the experimental data. The fitted lines are also included in Fig. 6. The data for 37Cu alloy was calculated according to this line; the results are presented in Table 4. As evident from Table 4, the calculated values agree well with the experimental values. These calculated values of  $k_0^{Exp}$  are used to model the microsegregation.

**3.4. Modeling results**

The results of microsegregation modeling are presented

in Fig. 7. In most cases, the calculations based on the experimental data show a better correlation with the

**Table 4. Results of  $k_0$  for 37Cu alloy**

Sample codes	$k_0$ by four different methods				Fitted value	Equilibrium value of $k_0$
	M1	M2	M3	M4		
37CuS1	0.34	0.22	0.17	—	0.19	0.12
37CuS2	0.36	0.20	0.22	0.20	0.20	0.12
37CuS3	0.35	0.11	0.31	0.27	0.25	0.13
37CuS4	0.30	0.07	0.33	—	0.36	0.16
37CuSF	—	—	0.46	0.46	0.43	0.17
37CuM1	0.61	0.50	0.15	—	0.17	0.12
37CuM2	0.37	0.22	0.20	0.20	0.17	0.12
37CuM3	0.20	0.07	0.20	—	0.19	0.13
37CuM4	0.18	0.05	0.28	—	0.23	0.16
37CuMF	—	—	0.27	0.42	0.26	0.17

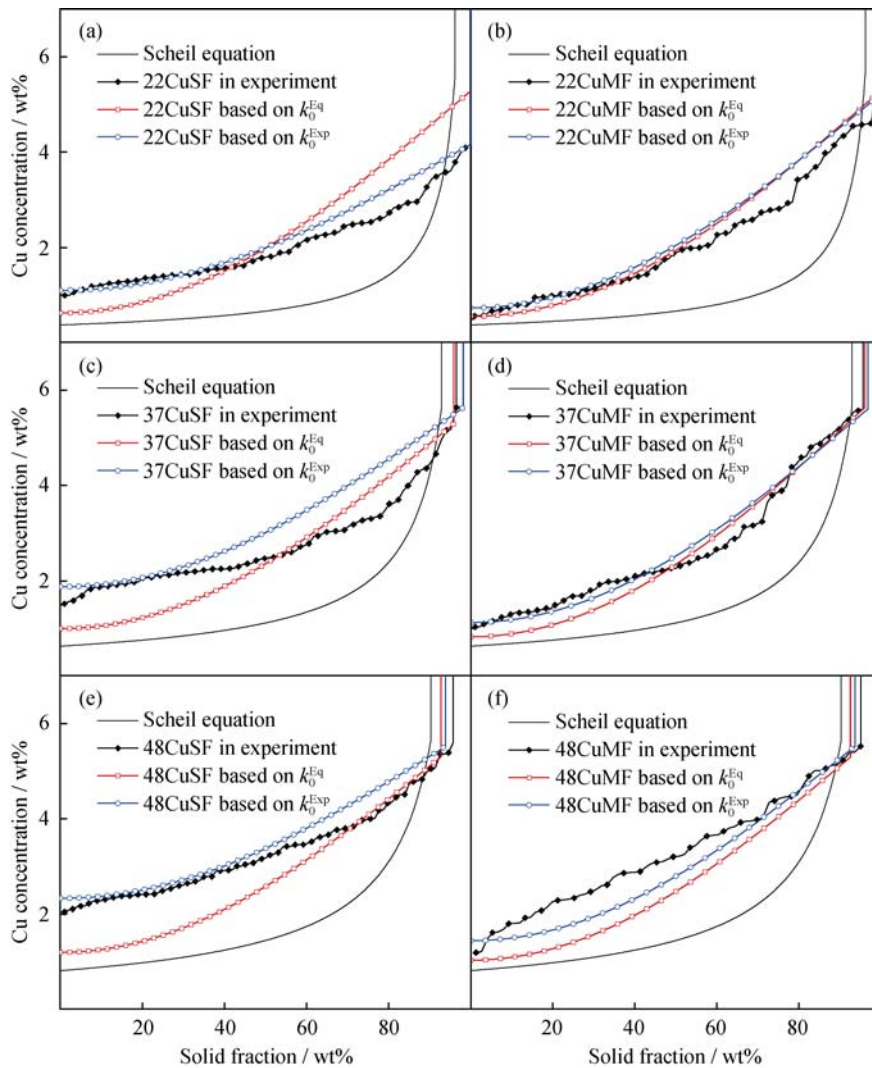


**Fig. 7. Calculated concentration profiles of microsegregation: (a) 22CuSF; (b) 22CuMF; (c) 37CuSF; (d) 37CuMF; (e) 48CuSF; (f) 48CuMF.**

experimental profile. At the cooling rate of  $0.5 \text{ K}\cdot\text{min}^{-1}$ , the use of  $k_0^{\text{Exp}}$  results in an overestimation of the experimental profile. This overestimation may be due to the effect of back diffusion in these samples, which affects the value of the experimental partition coefficient. Two main parameters that are widely used in the literature for the quantification of microsegregation are the minimum concentration of solute at the primary phase ( $C_{\text{min}}$ ) and the mass fraction of the non-equilibrium eutectic mixture ( $f_E$ ). According to Fig. 7, the concentration profile can not be calculated precisely; however,  $f_E$  and especially  $C_{\text{min}}$  can be accurately estimated. In most cases, the results calculated on the basis of  $k_0^{\text{Exp}}$  exhibit a better consistency with the experimental results. It can be concluded that the calculations based on  $k_0^{\text{Exp}}$  are more reliable than those based on  $k_0^{\text{Eq}}$ . As previously mentioned, some of the discrepancies between the calculations based on  $k_0^{\text{Exp}}$  and the experimental results can be due to the effect of back diffusion on the profile, which can cause the partition coefficient to be overestimated. Elucidation of this phenomenon requires the construction of a non-equilibrium phase diagram, which is currently underway in our lab and will be published later. It is believed that the exact value of  $k_0$  should lie between the equilibrium value and the experimental value measured in this study.

#### 4. Conclusions

(1) The methods that use the composition of solid (i.e., the minimum concentration or the concentration profile in the primary phase) are more reliable, and the partition coefficient values calculated by these methods agree well with each other.

(2) The experimental partition coefficient values (based on the minimum concentration or concentration profile in the primary phase) range from 0.15 to 0.59 and are greater than the values taken from the phase diagram (0.12 to 0.17).

(3) The calculation of concentration profile in the primary phase using experimental partition coefficients is more reliable than those based on the equilibrium partition coefficients.

#### Acknowledgements

The authors gratefully acknowledged the support by the Department of Casting of Metals, Royal Institute of Technology. One of the authors, M.H. Avazkonandeh-Gh., would like to thank the financial support by the Ministry of Sciences, Research and Technology, the Islamic Republic of

Iran, during his visit to the Royal Institute of Technology. The authors also thank Haji Muhhammad Muhmond and Saud Saleem for their assistance in setting up the experiments.

#### References

- [1] D.H. Kirkwood, Microsegregation, *Mater. Sci. Eng. A*, 65(1984), No. 1, p. 101.
- [2] I. Ohnaka, Mathematical analysis of solute redistribution during solidification with diffusion in solid phase, *Trans. ISIJ*, 26(1986), No. 26, p. 1045.
- [3] S. Kobayashi, Solute redistribution during solidification with diffusion in solid phase: a theoretical analysis, *J. Cryst. Growth*, 88(1988), No. 1, p. 87.
- [4] T. Kraft, M. Rettenmayr, and H.E. Exner, An extended numerical procedure for predicting microstructure and microsegregation of multicomponent alloys, *Modell. Simul. Mater. Sci. Eng.*, 4(1996), No. 2, p. 161.
- [5] X. Doré, H. Combeau, and M. Rappaz, Modelling of microsegregation in ternary alloys: application to the solidification of Al–Mg–Si, *Acta Mater.*, 48(2000), No. 15, p. 3951.
- [6] Q. Du and A. Jacot, A two-dimensional microsegregation model for the description of microstructure formation during solidification in multicomponent alloys: Formulation and behavior of the model, *Acta Mater.*, 53(2005), No. 12, p. 3479.
- [7] A. Turkeli, Approximate analytical models for microsegregation considering the effect of dendrite arm coarsening, *Mater. Sci. Forum*, 508(2006), p. 449.
- [8] S.N. Samaras and G.N. Haidemenopoulos, Modelling of microsegregation and homogenization of 6061 extrudable Al-alloy, *J. Mater. Process. Technol.*, 194(2007), No. 1-3, p. 63.
- [9] Q. Du, D.G. Eskin, A. Jacot, and L. Katgerman, Two-dimensional modelling and experimental study on microsegregation during solidification of an Al–Cu binary alloy, *Acta Mater.*, 55(2007), No. 5, p. 1523.
- [10] G. Kasperovich, T. Volkman, L. Ratke, and D. Herlach, Microsegregation during solidification of an Al–Cu binary alloy at largely different cooling rates (0.01 to 20,000 K/s): modeling and experimental study, *Metall. Mater. Trans. A*, 39(2008), No. 5, p. 1183.
- [11] J. Tang and X. Xue, Numerical simulation of multi-grain structure and prediction of microsegregation in binary Ni–Cu alloy under isothermal conditions, *Mater. Sci. Eng. A*, 499(2009), No. 1-2, p. 64.
- [12] T.P. Battle, Mathematical modelling of solute segregation in solidifying materials, *Int. Mater. Rev.*, 37(1992), No. 6, p. 249.
- [13] H. Fredriksson and U. Akerlind, *Solidification and Crystallization Processing in metals and Alloys*, John Wiley & Sons, Chichester, West Sussex, 2012, p. 475.
- [14] F.Y. Xie, T. Kraft, Y. Zuo, C.H. Moon, and Y.A. Chang, Mi-

- crostructure and microsegregation in Al-rich Al–Cu–Mg alloys, *Acta Mater.*, 47(1999), No. 2, p. 489.
- [15] H. Liang, T. Kraft, and Y.A. Chang, Importance of reliable phase equilibria in studying microsegregation in alloys: Al–Cu–Mg, *Mater. Sci. Eng. A*, 292(2000), No. 1, p. 96.
- [16] X.Y. Yan, F.Y. Xie, M. Chu, and Y.A. Chang, Microsegregation in Al–4.5Cu wt.% alloy: experimental investigation and numerical modeling, *Mater. Sci. Eng. A*, 302(2001), No. 2, p. 268.
- [17] E.C. Kurum, H.B. Dong, and J.D. Hunt, Microsegregation in Al–Cu alloys, *Metall. Mater. Trans. A*, 36(2005), No. 11, p. 3103.
- [18] M.N. Gungor, A statistically significant experimental technique for investigating microsegregation in cast alloys, *Metall. Trans. A*, 20(1989), No. 11, p. 2529.
- [19] J. Valdes, S.L. Shang, Z.K. Liu, P. King, and X.B. Liu, Quenching differential thermal analysis and thermodynamic calculation to determine partition coefficients of solute elements in simplified Ni-base superalloys, *Metall. Mater. Trans. A*, 41(2010), No. 2, p. 487.
- [20] W.F. Gale and T.C. Totemeier, *Smithells Metals Reference Book*, Elsevier, Burlington, 2004, p. 13.